JOURNAL OF COMPUTATIONAL PHYSICS 91, 344–360 (1990)

Electrical Impedance Tomography with Piecewise Polynomial Conductivities

THOMAS J. YORKEY

Lawrence Livermore National Laboratory, University of California, P.O. Box 808 L-496, Livermore, California 94550

Received April 28, 1988; revised October 30, 1989

Given only the static boundary flux and potential, electrical impedance tomography solves the inverse problem for the conductivity distribution. A Gauss–Newton solution is presented to solve this nonlinear problem when the conductivity distribution is represented by a piecewise polynomial basis function. An efficient method is presented to solve for the Jacobian matrix. This efficiency is made possible because of the local support of the basis functions used to approximate the conductivity distribution and data collection using the four-electrode technique. A method is presented for the local support case to solve for the Jacobian constants, which are needed to assemble the Jacobian matrix. It is shown that when higher than piecewise constant conductivities are desired it is more efficient to model conductivity than resistivity. Results are presented showing simulated reconstructions using a piecewise constant conductivity representation, and a (bi)linear conductivity representation with C^0 continuity across conductivity elements. These results show that although the Gauss–Newton method performs very well, further work needs to be done in designing meshes that increase the conditioning of the approximate Hessian matrix.

1. INTRODUCTION

Electrical impedance tomography (EIT) reconstructs a conductivity distribution from static electrical measurements on the object's periphery. In traditional computer tomography (CT) reconstruction, the probes are high-energy X rays with straight ray paths independent of the medium being probed. In contrast, the current paths and equipotential surfaces of EIT are functions of the unknown conductivity distribution. This unknown dependence leads to a nonlinear reconstruction problem in which questions of algorithmic convergence must be addressed. We propose a reconstruction algorithm based on an iterative linearization of the nonlinear relationship between the conductivity distribution and the electrical measurements.

The solution to the EIT problem has many applications. The biomedical community could use EIT as an imaging tool probing with nonionizing radiation. The EIT instrument can be made cheaply, on the order of a few thousand dollars, and operated with no harm to the patient. Although EIT is not a high-resolution imaging system, the data acquisition can be very fast, on the order of a millisecond.

0021-9991/90 $3.00

These facts suggest continuous bedside monitoring for such things as pulmonary edema, cerebral ventricular hemorrhage, and gastric emptying, to name a few.

EIT also has several geophysical applications. The most well-posed problem is in core sample analysis. Here a cylindrical section of earth is placed in a pressure vessel. The effects of various pressure and temperature conditions on the core can be visualized by displaying the conductivity as an image. EIT applications that suffer from illposedness are: half-plane resistivity surveys and borehole logging (the understanding of what materials lie beyond a borehole). The rapid data collection also suggests the study of rock failure under high stress.

In a practical application of EIT, we only have a finite amount of boundary information, which limits the degrees of freedom used to represent a conductivity distribution. With this limitation we wish to reconstruct a model as close to a realistic approximation as possible. A piecewise constant conductivity representation is most common; however, it may not have enough variation. We can apply a smoothing filter to the distribution before display, but a more formal treatment would be to model the conductivity with a higher order basis during the reconstruction. We discuss here how to reconstruct a conductivity model with a given order of basis functions.

Section 2 discusses the mathematics that describe the electrical fields governing EIT, and the numerical method that we use to approximate the solution. Section 3 shows the method we use to solve the inverse problem of EIT. Section 4 describes the numerical method we use to overcome the inherent illconditioning of the approximate Hessian matrix needed in the Gauss–Newton solution. Section 5 shows that the stiffness matrix used by the finite element method can be thought of as an electrical-network admittance matrix. Section 6 derives the numerical technique to efficiently calculate the Jacobian matrix needed in the Gauss–Newton solution. Section 7 shows how to calculate the constants needed in the efficient Jacobian matrix calculation. Section 8 discusses our particular implementation details for the results that Section 9 shows.

2. The Forward Problem

The equations that govern our measurements are

$$\begin{aligned} \nabla \cdot \sigma \nabla v &= 0, \qquad \text{in } \Omega; \\ \sigma \frac{\partial v}{\partial n} &= \gamma, \qquad \text{on } \partial\Omega, \end{aligned} \tag{1}$$

where σ is the conductivity distribution, which is everywhere real and positive, v the potential distribution, n the outward normal, γ the applied flux, Ω the domain of interest, and $\partial\Omega$ its boundary. For this paper we will be concerned with the two-dimensional problem, but the extensions to three dimensions are straightforward.

The solution to (1) is only known in closed form for relatively simple domains and conductivity distributions. When these simplifications are not valid, a numerical technique is used to approximate the solution. The finite-element method (FEM [1] is one such method.

The FEM divides Ω into a number of small elements and defines a basis function for v over these individual elements. The basis functions are typically Lagrange polynomials that have only local support. Since the operator $L = \nabla \cdot \sigma \nabla$ is self-adjoint we can use these same basis functions as the weighting functions, i.e., we can approximate (1) by the Galerkin method [2]. Since the basis functions are locally defined, we can assemble the FEM solution element-by-element, giving

$$Y\mathbf{v} = \mathbf{c}, \tag{2}$$

where Y is the global stiffness matrix, which is typically singular, $\mathbf{v}$ is a vector representing the potential distribution at the nodes of the elements, and $\mathbf{c}$ is the effective applied current at these nodes.

Section 5 shows that (2) represents some electrical network, although the physical parameters may be unrealizable (ex., negative resistors). Since (1) is a Neuman problem, v is determined only up to an additive constant. We make Y nonsingular by supplying this constant through a voltage reference node, forming a node-admittance matrix [3]. To supply a voltage reference node, let s be some node, then, set the sth row and column of Y equal to zero and the main-diagonal element to one. This new matrix is the constrained form of Y. Now set the sth entry of $\mathbf{c}$ to zero, grounding node s [4]. Then solve for $\mathbf{v}$.

3. The Reconstruction Algorithm

The FEM gives us a way of approximating the potential everywhere given the conductivity distribution and the appropriate boundary conditions. EIT wishes to solve the inverse problem; given the boundary conditions and the potential on the boundary, solve for the conductivity distribution. The difficulty in EIT is that the boundary potentials depend on any point in the conductivity distribution in a nonlinear way.

To solve this problem define:

1. $\mathbf{v}_0 \in R^n$, the n voltages we observe on the boundary.
2. $\mathbf{g} \subset D \in R^m$, a conductivity distribution with m degrees of freedom.
3. $\mathbf{f}: D \subset R^m \to R^n$, a function mapping a conductivity distribution with m degrees of freedom into a set of n approximate voltage observations.
4. $\phi = \frac{1}{2}(\mathbf{f} - \mathbf{v}_0)^{\mathrm{T}} (\mathbf{f} - \mathbf{v}_0)$, the squared error of the reconstruction.

Our problem in impedance imaging is finding a point $\mathbf{g}^*$ that is at least a local minima of the objective function ϕ. To solve this nonlinear problem, we use the

Gauss–Newton method [5, 6]. At iteration k with the estimate $\mathbf{g}^k$, we update our estimate of $\mathbf{g}^*$ to

$$\mathbf{g}^{k+1} = \mathbf{g}^k + \Delta\mathbf{g}^k,$$

where

$$\Delta\mathbf{g}^k = -[[\mathbf{f}']^T \mathbf{f}']^{-1} [\mathbf{f}']^T [\mathbf{f} - \mathbf{v}_0], \tag{3}$$

and $\mathbf{f}'$ is the total derivative of $\mathbf{f}$ with respect to $\mathbf{g}$, evaluated at $\mathbf{g}^k$. When the iteration step produces changes in the estimate of $\mathbf{g}^*$ that are smaller than some predetermined tolerance or correspondingly small changes in ϕ, we say the procedure has converged, and we stop.

If we observe at least m linearly independent voltages, the Jacobian matrix, $\mathbf{f}'$, will be of rank m. Then the approximate Hessian, $[\mathbf{f}']^T \mathbf{f}'$, will be of full rank, and since it is quadratic in form, it will also be positive definite. The fact that this iterative procedure produces an approximation to $\mathbf{g}^*$ is guaranteed by this positive definiteness. When we form $\mathbf{v}_0$ in the presence of additive zero-mean independent noise, the Gauss–Newton method is known as nonlinear least-squares estimation, which converges in distribution [7].

4. Ill-conditioning

We found $[\mathbf{f}']^T \mathbf{f}'$ ill-conditioned. Our particular measurement scheme made the sensitivity to the conductivity farthest from the boundary much worse. To reduce measurement error, we use the four-electrode method [8]. We kept our current source leads on adjacent electrodes and similarly with our voltage measurement leads. An optimization for electrode-lead positions may result in better conditioning of $[\mathbf{f}']^T \mathbf{f}'$ [7, 9].

To overcome the ill-conditioning we used the Marquardt method [10]. The Marquardt method forms

$$(A + \lambda I_m)\mathbf{z} = \mathbf{b} \tag{4}$$

for some scalar λ, where A is the normalized matrix of $[\mathbf{f}']^T \mathbf{f}'$, $\mathbf{b}$ the normalized vector of $[\mathbf{f}']^T (\mathbf{f} - \mathbf{v}_0)$, and I_m is the $m \times m$ identity matrix. It solves for $\mathbf{z}$ and obtains its unnormalized form, $\Delta\mathbf{g}^k$. Then decreases λ by 10 if $\phi^{k+1} < \phi^k$ or continuously increases it by 10 until $\phi^{k+1} < \phi^k$. When the distance between $\mathbf{g}^k$ and $\mathbf{g}^*$ is small, λ is small, and (4) becomes (3). When the distance is large, λ is large and (4) essentially turns the correction vector into the negative direction of the gradient of ϕ, decreasing the amount of correction made. For a small enough correction, this modified direction is guaranteed to decrease ϕ. Marquardt suggested starting with $\lambda = 0.01$. The ill-conditioning was so large we started with $\lambda = 0.1$.

5. Stiffness Matrix Analogy

In the next section, it will prove advantageous to develop the analogy between (2), and the representation of an electrical network. We now show that although not always physically realizable, the assembled FEM represents a general electrical network [11, 12]. If we generalize conductors to be both positive and negative valued, then the constraints left on a network are that it satisfy reciprocity and Kirchoff's laws.

The (i, j)th entry in the stiffness matrix is calculated from

$$y_{ij} = \int_{\Omega} \sigma \nabla \varphi_i \cdot \nabla \varphi_j \, d^2x, \tag{5}$$

where, for example, φ_i is the basis function for node i. Since the basis functions are dimensionless, y_{ij} has the dimensions of siemens, the same as a network admittance matrix. Equation (5) easily shows that the stiffness matrix is symmetric, as is the network admittance matrix. This symmetry guarantees reciprocity.

To satisfy Kirchoff's laws, the admittance matrix must sum to zero along any column or row. To see that this holds for Y we use the fact that for φ_i being Lagrange polynomials for all i, then

$$\sum_i \varphi_i = 1$$

everywhere in Ω [13]. Therefore, for the ith row,

$$\begin{aligned} \sum_i y_{ij} &= \sum_i \int_{\Omega} \sigma \nabla \varphi_i \cdot \nabla \varphi_j \, d^2x \\ &= \int_{\Omega} \sigma \nabla \sum_i \varphi_i \cdot \nabla \varphi_j \, d^2x \\ &= 0. \end{aligned}$$

By symmetry in (5) any jth column must also sum to zero.

6. An Efficient Way of Calculating the Jacobian Matrix

To calculate the Jacobian matrix, one needs to calculate $\partial \mathbf{v}/\partial \mathbf{g}$, which from (2) is

$$\frac{\partial \mathbf{v}}{\partial \mathbf{g}} = -Y^{-1} \frac{\partial Y}{\partial \mathbf{g}} Y^{-1} \mathbf{c},$$

where, of course, we have used the constrained form of Y. We show here how to use the network compensation theorem to efficiently calculate the Jacobian matrix when using the four-electrode method. Yorkey *et al.* [5] showed by example that for the four-electrode method the compensation theorem procedure is more efficient than directly implementing the above equation. Recently Isaacson [9] has proposed an l-electrode method, where current is applied to l electrodes. For this generalization it is more efficient to use the above equation directly to calculate the Jacobian matrix.

Figure 1 shows the setup. Apply a current source to port k, c_k, resulting in the voltage v_i at port i. If the port j conductance, y_j, changes to $y_j + \Delta y_j$, [14, 15] showed that the voltage change at port i is

$$\Delta v_i = -c_k \, \Delta y_j \, z_{ij'} z_{kj}, \tag{6}$$

where, for example, z_{ij} is the transfer impedance between ports i and j, and j' denotes the new port formed by Δy_j. If y_j is the jth conductance defined in our FEM solution then we can use (6) to help form a Jacobian matrix entry.

Section 7 will show that for a polynomial representation of σ, the jth degree of freedom in this conductivity representation contributes to L conductor values $y_{j(1)} \cdots y_{j(L)}$ by

$$y_{j(l)} = \alpha_{j(l)} + s_{j(l)} \, g_j,$$

where $\alpha_{j(l)}$ is the contribution from other degrees of freedom, and $s_{j(l)}$ is a constant. The number of conductors effected by the jth degree of conductivity freedom, L, may be a function of j, but we prefer the simplier notation. Because of the importance of $s_{j(l)}$, we call them the Jacobian constants for the degree of freedom index j. A change in g_j alone leads to

$$\Delta y_{j(l)} = s_{j(l)} \, \Delta g_j.$$

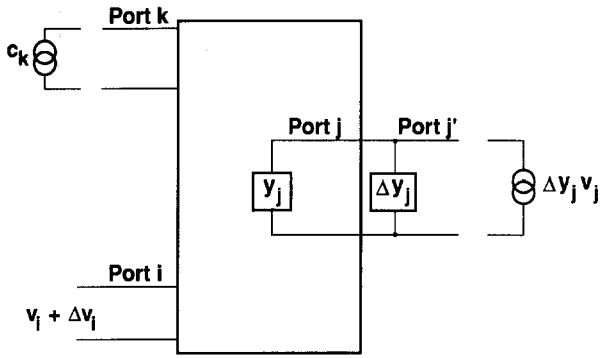

FIG. 1. When we apply a current source to port k and an admittance y_j changes to $y_j + \Delta y_j$ the compensation theorem shows us how to calculate the resulting change in voltage at port i by removing the current source and applying a particular current source to port j'. We can use this theorem to calculate the Jacobian matrix more efficiently.

By repeated application of (6), the voltage change due to a conductance change in L ports is

$$\Delta v_i = -c_k \sum_{l=1}^{L} \Delta y_{j(l)} z_{ij(l)'} z_{kj(l)}.$$

Therefore a change in the conductivity of one degree of freedom leads to

$$\Delta v_i = -\Delta g_j c_k \sum_{l=1}^{L} s_{j(l)} z_{ij(l)'} z_{kj(l)}.$$

Dividing by Δg_j and letting $\Delta g_j \to 0$, we obtain

$$\frac{\partial v_i}{\partial g_j} = -c_k \sum_{l=1}^{L} s_{j(l)} z_{ij(l)} z_{kj(l)}.$$

Note we no longer need j' because now $z_{ij'} = z_{ij}$. If $c_k = c$ for all k, and using $z = v/c$, then

$$\frac{\partial v_i}{\partial g_j} = -\frac{1}{c} \sum_{l=1}^{L} s_{j(l)} v_{ij(l)} v_{kj(l)}, \tag{7}$$

which is the (i, j)th entry in the Jacobian matrix.

To use (7), measure $v_{kj(l)}$ for the L branch voltages with current source at that port k which corresponds with the ith measurement. Then place the current source at that port corresponding to the ith measurement and measure $v_{ij(l)}$, the L branch voltages again. Then multiply and sum these terms according to (7).

7. Calculation of the Jacobian Constants

We present here a method to calculate the constants needed in (7) to form the Jacobian matrix efficiently. The (i, j)th element in Y is defined as

$$y_{ij} = \int_{\Omega} \sigma \nabla \varphi_i \cdot \nabla \varphi_j \, d^2x.$$

Let us assume the σ can be approximated by

$$\sigma = \sum_{\beta} p_\beta g_\beta$$

for some spatially dependent parameters p, and degrees of freedom β. Then,

$$y_{ij} = \int_{\Omega} \left[\sum_{\beta} p_\beta g_\beta \right] \nabla \varphi_i \cdot \nabla \varphi_j \, d^2x = \sum_{\beta} g_\beta \int_{\Omega} p_\beta \nabla \varphi_i \cdot \nabla \varphi_j \, d^2x. \tag{8}$$

Since g_β is not a function of the integration, we can take the derivative of (8) with respect to a particular degree of freedom, g_β,

$$\frac{\partial y_{ij}}{\partial g_\beta} = \int_\Omega p_\beta \nabla_i \cdot \nabla \varphi_j \, d^2x. \tag{9}$$

It is important to keep straight the fact that the value of the admittance that connects node i to node j is $-y_{ij}$. This subtlety comes about because the current is defined as positive inward. So we will define the Jacobian constants as the negative of the right-hand side of (9),

$$\frac{\partial y_{ij}}{\partial g_\beta} = -s_{\beta(l)},$$

for some l.

Comparing (8) with (9), we can define the procedure for finding $s_{\beta(l)}$. Assemble the stiffness matrix for g_β equaling one for a particular β and zero elsewhere. Since Y is symmetric, the nonzero off-diagonal entries in either the lower or upper triangular segments of Y are the negative $s_{j(l)}$'s. The number of these entries is L. If, for a particular β, we index the L admittance values that these nonzero entries correspond to by $\beta(l)$, then we can write

$$\frac{\partial y_{\beta(l)}}{\partial g_\beta} = s_{\beta(l)},$$

or by integrating with respect to g_β,

$$y_{\beta(l)} = \alpha_{\beta(l)} + s_{\beta(l)} g_\beta.$$

This is the form Section 6 needed.

Note that, since (9) is independent of the conductivity distribution, it need only be evaluated once in the reconstruction process. If instead we wished to take derivatives of an interpolated resistivity distribution,

$$\rho = \frac{1}{\sigma} = \sum_\beta p_\beta r_\beta.$$

Then (9) would become

$$\frac{\partial y_{ij}}{\partial r_\beta} = -\int_\Omega \left[\frac{1}{\sum_\beta p_\beta r_\beta} \right]^2 p_\beta \nabla \varphi_i \cdot \nabla \varphi_j \, d^2x, \tag{10}$$

which is a function of the resistivity distribution, and therefore would need evaluation at each iteration. If the distribution were piecewise constant, then (10) would simplify to

$$\frac{\partial y_{ij}}{\partial r_\beta} = -\frac{1}{r_\beta^2} \int_\Omega p_\beta \nabla \varphi_i \cdot \nabla \varphi_j \, d^2x, \tag{11}$$

where p_β acts as a window over which the integration is performed. In this case, we would obtain for (7)

$$\frac{\partial v_i}{\partial r_j} = \frac{1}{cr_j^2} \sum_{l=1}^{L} s_{j(l)} v_{ij(l)} v_{kj(l)}.$$

The integrand in (11) is independent of the resistivity distribution, and therefore need only be calculated once.

8. Implementation

In order to maintain a reasonable potential calculation, the FEM mesh must be dense where the voltage gradient is high. For implementation ease, we would like the conductivity degrees of freedom to correspond independently to each element in the mesh. However, we are limited to m degrees of freedom in our conductivity model, and oftentimes this number is not large enough to provide a reasonable mesh and also adequantely solve for the potential. To circumvent this problem define two meshes, one dense mesh for accurate calculation of the potentials, and one for the conductivity distribution.

Although not necessary in the previous sections, it proves convenient to have the conductivity mesh a subgraph of the potential mesh. This method keeps C^∞ continuity of the conductivity distribution within each potential-mesh element, and therefore allows numerical integration to be exact without further subdivision.

This subgraph goal sometimes becomes impossible to achieve near the boundary. If the isoparametric elements are of a lower order than the boundary itself then the coarse conductivity mesh will not interpolate the boundary as well as the fine potential mesh. Figure 2 shows an example for a piecewise linear interpolation to a curved boundary with (bi)linear elements. The extrapolation of the conductivity values outside of its course mesh is a reasonable approach since the amount of extrapolation is so small.

9. Results

We present now two examples of polynomial conductivity elements, piecewise constant, and piecewise (bi)linear. We simulated a two-dimensional unit-radius inhomogeneous conductivity distribution. We used 16 electrodes equally spaced on the objects boundary. We were able to simulate $n = 104$ independent measurements. For the examples shown, the starting estimate was the average of the actual distribution.

Figure 3 shows the potential mesh we used to model this system. The elements outside the circle are used to model the effects of the electrodes. We have found experimentally that this mesh is fine enough to obtain results within 10% of actual,

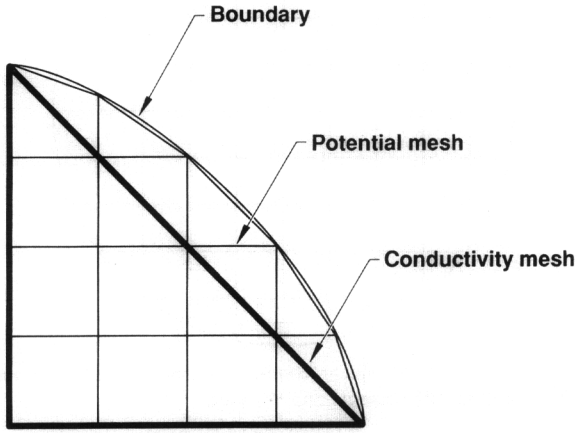

FIG. 2. When fitting a domain with lower order basis functions than the boundary, an exact subgraph cannot be defined. In this example the boundary is a sector from a circle. The potential mesh is piecewise (bi)linear, using linear triangles at the boundary. The conductivity is a coarse corresponding to the big linear triangle.

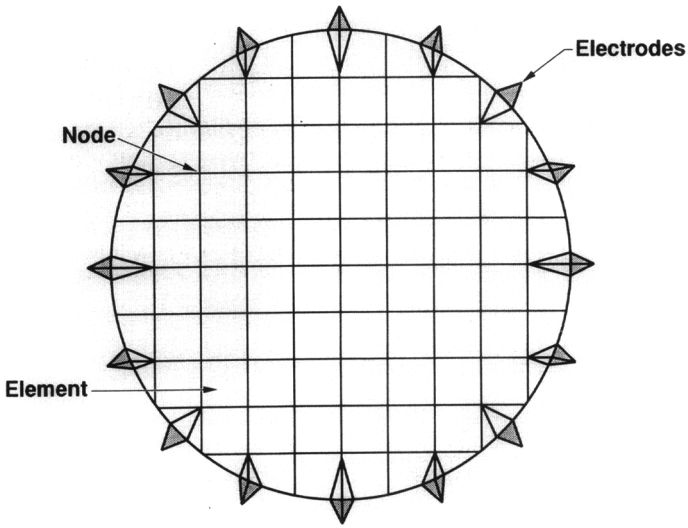

FIG. 3. The piecewise (bi)linear potential mesh modeling a circular domain. The elements outside the circle are given very high conductivity values to model the electrode effects. The electrode conductivities are assumed known, and therefore not solved for in the inverse problem. There are 124 elements and 129 nodes within the mesh. The conductivity is defined on a subgraph of this mesh.

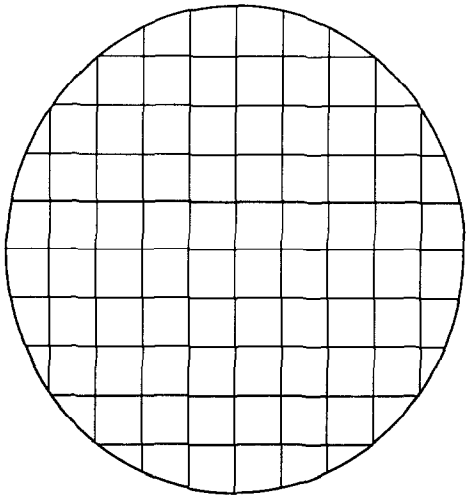

FIG.4. The piecewise constant or (bi)linear conductivity mesh; except for the boundary a simple subgraph of Fig. 3. This mesh has 89 elements and 94 nodes.

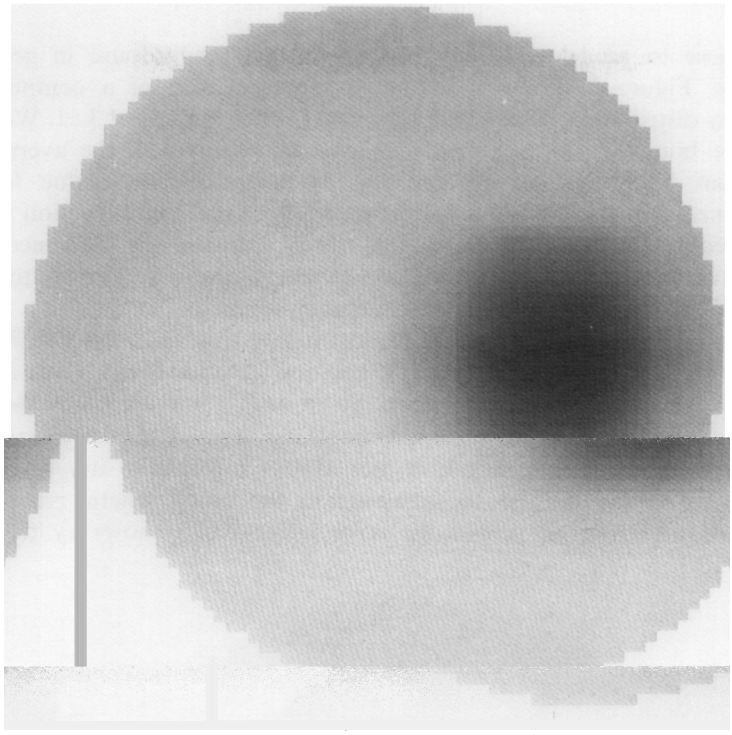

FIG 5. A smoothed image from a piecewise constant resistivity model using the mesh from Fig. 4. Resistivity increases with darkness. The maximal resistivity contrast was 3 : 1. The resistivity model had 89 degrees of freedom.

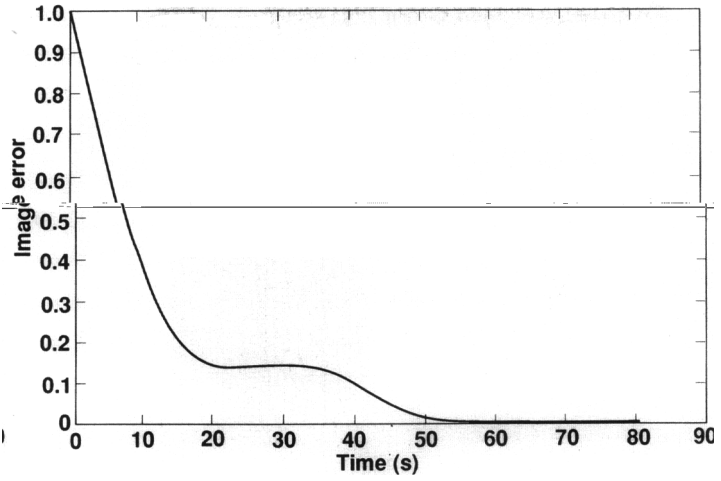

FIG. 6. A cubic spline fit to the image error at each iteration verses CPU time on a VAX 11/785. One iteration equals approximately 11 s.

which is good enough for the examples. Note that there are 124 elements and 129 nodes within the circle, so we cannot use this mesh to define the conducitivity for either a piecewise constant or (bi)linear variation since $n = 104$.

Figure 4 shows the conductivity mesh. Except for the boundary, this mesh is a trivial subgraph of Fig. 3. The conductivity mesh has 89 elements and 94 nodes, so we can use it for either a piecewise constant or (bi)linear representation.

For our first example, we will use a piecewise constant resistivity representation.

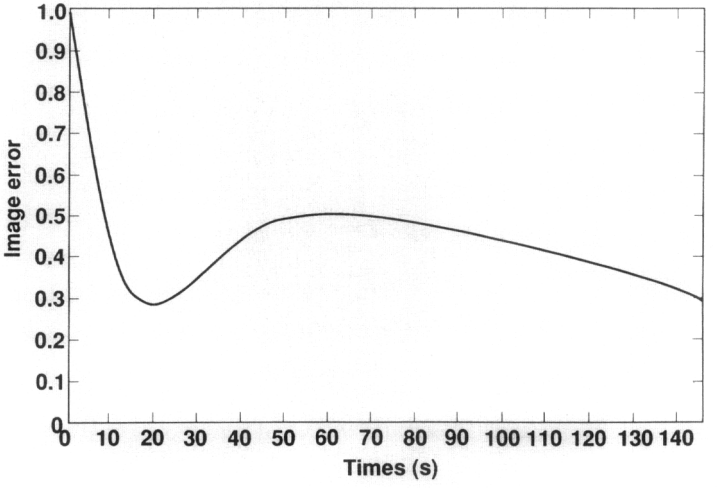

FIG. 7. The image error when the anomaly in Fig. 5 is centered. Note the difficulty in reconstruction.

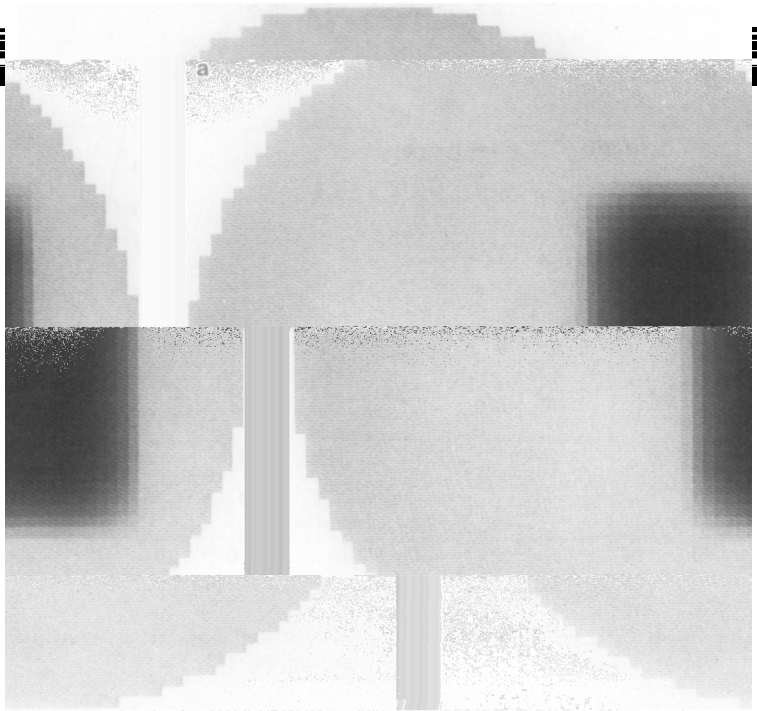

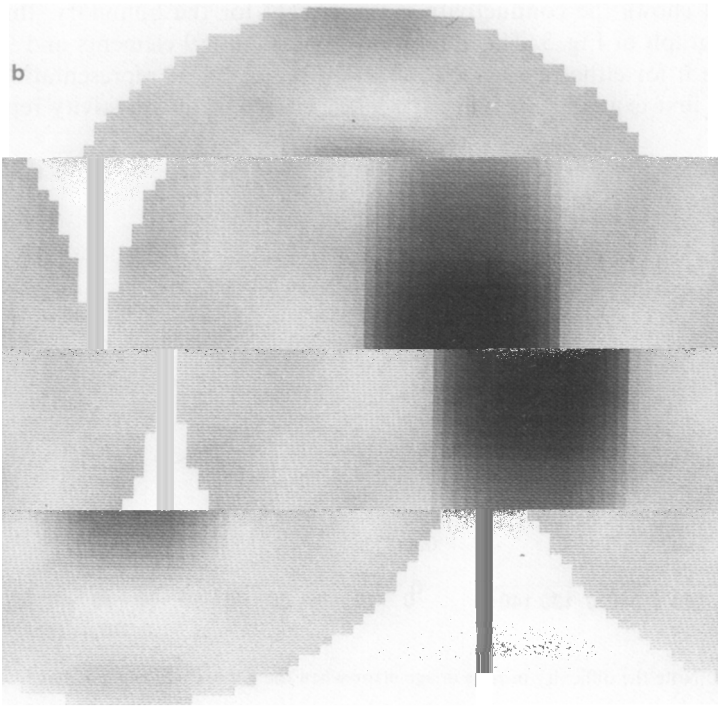

FIG. 8. The final images corresponding to: (a) Fig. 6; (b) Fig. 7.

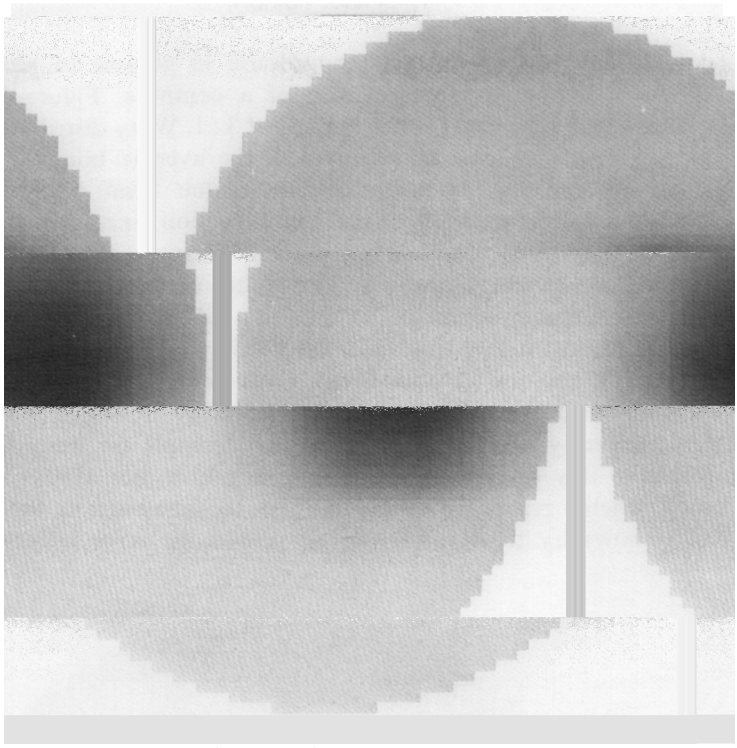

FIG. 9. A piecewise (bi)linear conductivity distribution with 94 degrees of freedom. Now conductivity increases with darkness. The maximal conductivity contrast was 3 : 1. This smooth image is not artificial as it is in Figs. 5 and 8.

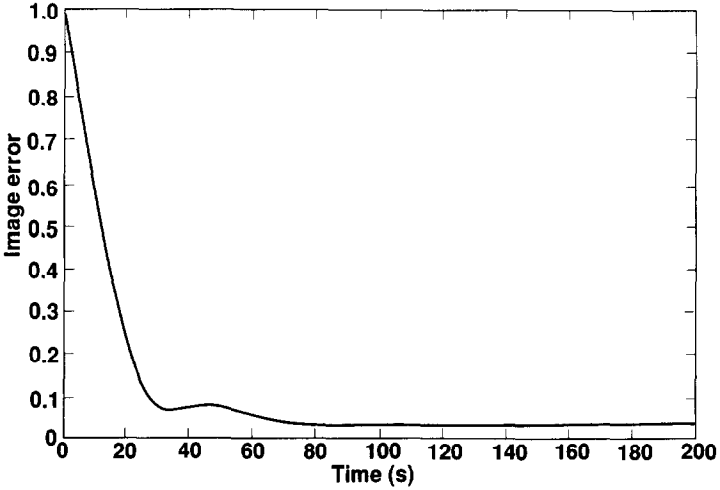

FIG. 10. The image error in reconstructing Fig. 9. The increase in the degrees of freedom and the order in the conductivity basis have increased the reconstruction time from 11 s per iteration to 22 s.

We choose to model resistivity because of its standard use in geophysics and medicine. Figure 5 shows a smoothed representation of a computer-simulated resistivity distribution, which had a maximal contrast ratio of 3 : 1. We assume that from the boundary measurements at least an estimate of the average resistivity value can be found, so we use the average resistivity value for an initial homogeneous guess. To estimate the accuracy of the reconstruction we define the error measure at any iteration step as the L_2 norm of the difference between the true distribution and the estimated one at that iteration divided by the L_2 norm of this difference with the initial guess, quantity squared.

Figure 6 shows this error versus reconstruction time on a VAX 11/785. The error was interpolated by a cubic spline in between iteration steps. Each iteration took approximately 11 s of computer time. So in only a few iterations the image error was very small. Although for this example we were able to recover the original anomaly to any degree of accuracy, it is not always possible to iterate to such a small error. By simply moving the anomaly to the center where there is less sensitivity to its presence, we obtain the error curve Fig. 7 shows. The lack of

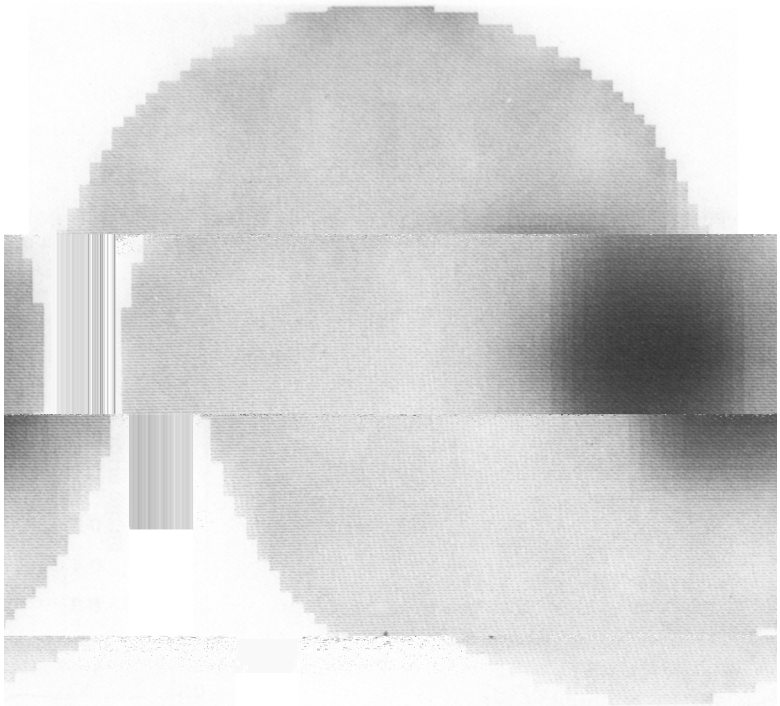

FIG. 11. The final image corresponding to Fig. 10.

sensitivity to even this large anomaly caused the reconstructed image to overshoot the true resistivity. Figure 8 shows the final reconstruction for both these cases.

Our second example is a piecewise (bi)linear representation. Figure 9 shows a piecewise (bi)linear interpolation of a conductivity

$$\sigma(x, y) = 1 + 2 \exp\left[-\frac{(x - x_0)^2 + y^2}{r_0^2} \right]$$

for $x_0 = 0.5$ and $r_0 = \sqrt{0.05}$. Now the smooth image is not artificial. This distribution gives also gives a maximal contrast of 3 : 1. Figure 10 shows the error curve, where the time per each iteration has almost doubled. This time result is predominantly caused by the fact that the number of degrees of freedom in the conductivity mesh increased from 89 to 94. Since the calculation of (3) is $O(m^3)$, this increase in freedom results in a tremendous increase in computing time. Figure 10 shows that although the final image-error converged to some small value, the error did not become negligible small. Figure 11 shows the final image.

10. Conclusions

With EIT we have only a finite amount of boundary information, which limits the degrees of freedom used to represent a conductivity distribution. With this limitation we wish to reconstruct a model as close to a realistic approximation as possible. Often times a piecewise constant conductivity representation may not have enough variation. We can artificially smooth the distribution before display, but a better treatment is to model the conductivity with a higher order basis in the reconstruction, as has been shown.

With the method outlined here, a continuous conductivity distribution can be adequately modeled and computed with any order basis desired. If we describe the potential and conductivity distributions by Lagrange polynomials, then the derivatives needed of the estimated voltages are easy to calculate. When we use a (bi)linear or higher order of basis for the conductivity, we can reduce the complexity of these calculations by interpolating conductivity values rather than resistivities. These numerical implementation techniques result in saving time in both algorithm development and execution of the code.

Results like those of Figs. 7 and 10 have led us to believe that although the Gauss–Newton method quickly iterates to an estimate of $\mathbf{g}^*$, this minima may only be a local one. Since this work involved computer simulations with double precision arithmetic, our noise level was low. Our boundary measurements formed a linear basis set for any other boundary measurements. So the measurements had all the information in them that any other measurement scheme would have. It is for these reasons that we believe our inability to converge to a neglible error was due to suboptimal conductivity meshes. Perhaps the mesh should become less dense farther from the boundary. More thorough analysis of the reconstruction problem

for a given conductivity basis function may show how to better design a reconstruction mesh to minimize the effects of local minima.

With real data there will be appreciable noise levels. Then there will be some measurements schemes that provide more information than others. These noise effects should be diminished by more optimal probing techniques [9]. It is not hard to believe that ones ability to distinguish two different conductivity distributions can improve if current is applied an more than just two electrodes.

ACKNOWLEDGMENTS

Work performed under the auspices of the U.S. Department of Energy by the Lawrence Livermore National Laboratory under Contract W-7405-ENG-48 and supported specifically by the Geosciences Research Program directed by the DOE Office of Energy Research within the Office of Basic Energy Sciences, Division of Engineering and Geosciences.

REFERENCES

1. P. TONG AND J. N. ROSSETTOS, *Finite-Element Method: Basic Technique and Implementation* (MIT Press, Cambridge, MA, 1977).
2. R. F. HARRINGTON, *Field Computation by Moment Methods* (Krieger, New York, 1969).
3. C. A. DESOER AND E. S. KUH, *Basic Circuit Theory* (McGraw–Hill, New York, 1969).
4. S. K. MITRA, *Analysis and Synthesis of Linear Active Networks* (Wiley, New York, 1969).
5. T. J. YORKEY, J. G. WEBSTER, AND W. J. TOMPKINS, *IEEE Trans. Biomed. Eng.* **BME-34**, 843 (1987).
6. J. M. ORTEGA AND W. C. RHEINBOLT, *Iterative Solutions of Nonlinear Equations in Several Variables* (Academic Press, New York, 1970).
7. G. E. P. BOX AND H. L. LUCAS, *Biometrika* **46**, 77 (1959).
8. J. G. WEBSTER (Ed.), *Medical Instrumentation: Application and Design* (Houghton Mifflin, Boston, 1978).
9. D. ISAACSON, *IEEE Trans. Med. Imaging* **MI-5**, 91 (1986).
10. B. W. MARQUARDT, *SIAM J. Appl. Math.* **11** 431 (1963).
11. O. C. ZIENKIEWICZ, *The Finite Element Method* (McGraw–Hill, London, 1971).
12. R. D. COOK, *Concepts and Applications of Finite Element Analysis*, 2nd ed. (Wiley, New York, 1981).
13. J. STOER AND R. BULIRSCH, *Introduction to Numerical Analysis* (Springer-Verlag, New York, 1980).
14. T. MURAI AND Y. KAGAWA, *IEEE Trans. Biomed. Eng.* **BME-32**, 177 (1985).
15. K. NAKAYAMA, W. YAGI, AND S. YAGI, in *Proc. 5th Int. Conf. Elect. Bio-Impedance, 1981*, p. 99, Tokyo, Japan, 1981.